

# SYNTHESIS OF PURE NANOCRYSTALLINE MAGNESIUM SILICATE POWDER

F. TAVANGARIAN, R. EMADI

Department of Materials Engineering, Isfahan University of Technology (IUT),  
Isfahan 84156-83111, Iran

E-mail: f\_tavangarian@yahoo.com

Submitted January 1, 2010; accepted February 15, 2010

**Keywords:** Magnesium Silicate; Nanomaterials; Mechanical Activation, Ceramics

*Pure nanocrystalline forsterite ( $Mg_2SiO_4$ ) powder was synthesized by mechanical activation technique followed by subsequent annealing. The starting materials were talc [ $Mg_3Si_4O_{10}(OH)_2$ ], magnesium carbonate ( $MgCO_3$ ), and magnesium oxide ( $MgO$ ) powders. To produce forsterite, two mixtures were prepared including talc and magnesium carbonate (first mixture) as well as talc and magnesium oxide powders (second mixture). First, both mixtures were milled by a planetary ball mill, and then annealed at 1000 and 1200° C for 1 h. Differential thermal analysis (DTA), X-ray diffraction (XRD), atomic absorption spectrometry (AAS), transition electron microscopy (TEM), and scanning electron microscopy (SEM) techniques were utilized to characterize the initial and synthesized powders. A pure nanocrystalline forsterite with a mean crystallite size of 40 nm was obtained after 10 h ball milling of the first mixture and subsequent annealing at 1000 °C for 1 h. On the contrary, after 5 h of mechanical activation of the second mixture and subsequent annealing at 1000° C for 1 h, pure nanocrystalline forsterite was synthesized with 60 nm mean crystallite size.*

## INTRODUCTION

Mechanical activation has been widely used to synthesize a variety of materials such as nanocrystalline materials [1], intermetallic compounds [2], and composites [3, 4]. Roughly, in all cases, the final product has nanosize structure which exhibits better properties and performance in comparison to the conventional coarse-grain materials [5]. Chemical reactions induced by mechanical treatment, i.e. mechanochemical synthesis, are known to be very effective for preparing nanocrystalline powders consisting of more than two phases [6].

Forsterite is a crystalline magnesium silicate ceramic with chemical formula  $Mg_2SiO_4$ . It is a member of olivine family of crystals [7]. Forsterite builds on silica tetrahedron with about 55 % of covalent bonding. Hence, it is expected to have low dielectric constant ( $\epsilon_r = 6.8$ ) and it is suggested as a suitable dielectric material for millimeter-wave communication [8]. Moreover, it shows good refractoriness with high melting point (1890° C), low thermal expansion, good chemical stability and excellent insulation properties even at high temperatures [9-11]. The manufacturers of the SOFC (solid oxide fuel cells) find forsterite interesting due to its linear thermal expansion coefficient, perfectly matching the other cell components, and also for its very high stability in fuel cell environments [7, 10].

Several methods including heating  $MgO$  and  $SiO_2$  powders (up to 1525°C) [12], co-precipitation [13], and sol-gel techniques have been employed to prepare pure forsterite [14-17]. During the synthesis of forsterite, it is very difficult to avoid the formation of  $MgSiO_3$  or/and  $MgO$ , and thermal treatments up to 1200-1600°C are necessary to obtain pure forsterite. Enstatite ( $MgSiO_3$ ) dissociates into forsterite and a  $SiO_2$ -rich liquid at 1557° C [10].

The main point in synthesizing forsterite ceramics involves provisions to avoid the appearance of  $MgSiO_3$  and  $MgO$  secondary phases. As pure forsterite is hard to produce, the aim of the present work is to develop a well controlled and economical method for the synthesis of single-phase nanocrystalline forsterite powder from talc,  $MgCO_3$ , and  $MgO$  and to evaluate the effect of  $CO_2$  in  $MgCO_3$  on the synthesis of forsterite powder.

## EXPERIMENTAL

### Powder preparation

Talc ( $Mg_3Si_4O_{10}(OH)_2$ ) (98% purity, Merck), magnesium carbonate ( $MgCO_3$ ) (98% purity, Aldrich), and periclase ( $MgO$ ) (98% purity, Merck) powders with mean particle size of 20, 10 and 5  $\mu m$  respectively, were used as starting materials. Two mixtures were prepared to study

the reaction of forsterite formation. The first mixture was prepared by mixing magnesium carbonate and talc powders with molar ratio of 5:1 to obtain stoichiometric forsterite (Mix 1). To evaluate the effect of CO<sub>2</sub> in the form of magnesium carbonate on the forsterite reaction rate, the second mixture was prepared on the basis of periclase and talc powders with molar ratio of 5:1 (Mix 2).

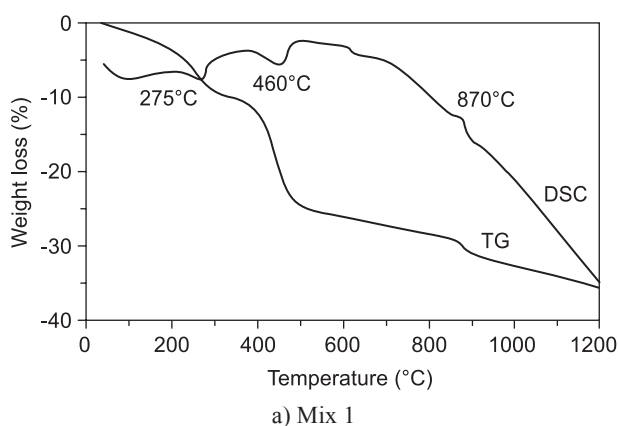
Two mixtures were then milled in a planetary ball mill (Fritsch P7 type) under ambient conditions, separately. The milling media consisted of a hardened steel vial (125 ml) with five balls 20 mm in diameter (each weighing 32.5 gr). In all milling runs, the ball-to-powder weight ratio was 10:1 and the rotational speed of the main disc was set at 500 rpm. Maximum milling time was 10 h. Heat treatment was carried out at 1000 and 1200°C for 1 h.

#### Powder characterization

Differential thermal analysis (DTA) was performed on as-milled powders in order to observe any exothermic peaks, which would indicate crystallization temperatures of forsterite. Weight losses during temperature increase were measured using thermogravimetric analysis (TG) in the temperature range from room temperature to 1200°C in air and at a heating rate of 10°C/min. A Philips X'PERT MPD diffractometer with Cu K $\alpha$  radiation ( $\lambda = 0.154056$  nm) was used for X-ray diffractometry (XRD) analysis in order to investigate heat treatment as well as phase transformation during the reactions. XRD patterns were recorded in the  $2\theta$  range of 20–80° (step size of 0.04° and time per step of 1 s). The crystallite size of forsterite powder was calculated from the XRD patterns using the Williamson-Hall approach [18]:

$$\beta \cos \theta = \frac{K\lambda}{D} + 2A\sqrt{\epsilon^2} \sin \theta \quad (1)$$

where  $\theta$  is the Bragg diffraction angle,  $D$  is the crystallite size,  $\epsilon$  is the average internal strain,  $\lambda$  is the wavelength of the radiation used,  $\beta$  is the diffraction peak width at half maximum intensity,  $K$  is the Scherrer constant (0.91)



and  $A$  is the coefficient which depends on the distribution of strain; it is near to unity for dislocations.

The morphology of powder particles was observed by scanning electron microscopy (SEM) in a Philips XL30 at an acceleration voltage of 30 kV and the image analysis method was used to measure forsterite powder particles. A Perkin-Elmer atomic absorption spectrometer (Model 2380) was used to determine iron and chromium contamination introduced in a 10 h milled sample. Transmission electron microscopy (TEM; Leo 912AB) technique was utilized to characterize the morphology and nanostructure of the synthesized forsterite powder.

## RESULTS AND DISCUSSION

### Thermal analysis

Figure 1 shows TG and DSC traces of powders after 1 h of ball milling of Mix 1 and 2, respectively. As can be seen in Figure 1a, the weight loss of ball milled powder of Mix 1 occurred in three main stages. The first stage ( $T < 300^\circ\text{C}$ ) was due to the loss of hydration water. The second stage occurred between 300 - 500°C as a result of decomposition of magnesium carbonate and crystallization of MgO. The third stage was from 500°C to 1200°C could be due to the liberation of structural water of talc. DSC traces exhibited two strong endothermic peaks at 275°C and 460°C and one small exothermic peak at 870°C. These three peaks can be attributed to the dehydration of powders, the calcination of MgCO<sub>3</sub> and the formation of forsterite structure, respectively [19]. In comparison to Figure 1a, just the second stage was disappeared in Figure 1b, which is due to the lack of CO<sub>2</sub> in second mixture.

### XRD analysis

Figure 2 shows the XRD patterns of powders of Mix 1 and 2 after different ball milling times, respectively. As can be seen in Figure 2a, Milling of the first powder mixture (Mix 1) for 5 h led to the broadening of XRD

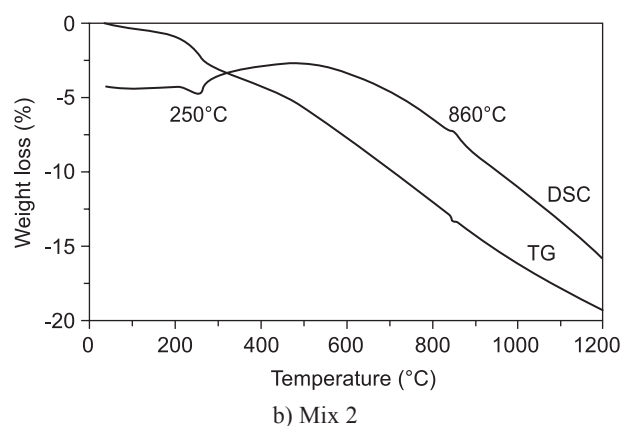


Figure 1. TG and DSC traces of powder obtained after 1 h of mechanical activation.

peaks and a significant decrease in their intensities. By increasing the milling time up to 10 an amorphous structure developed on XRD patterns. On the contrary, ball milling of second powder mixture (Mix 2) could not create amorphous structure and MgO peaks still persisted after 10 h of milling.

In order to produce forsterite powder, the milled powders were annealed at 1000 and 1200°C for 1 h. Figure 3 and 4 show the structure of samples after heat treatment. As can be seen in Figure 3a, Annealing of sample milled for 5 min (Mix 1) led to the complete vanishing of talc. Additionally strong periclase XRD peaks (XRD JCPDS data file No. 43-1022) were appeared on XRD trace. Traces of enstatite (XRD JCPDS data file No. 11-0273) and forsterite (XRD JCPDS data file No. 34-0189) were also observed at this

stage. As can be seen in Figure 3a for samples milled for longer times, the fraction of forsterite phase increased after annealing while the periclase as well as enstatite fractions content reduced so that for sample milled for 10 h only the forsterite phase can be detected on XRD trace. Detailed analysis of the changes of the MgO diffraction line intensities is one of the possible parameters for describing the reaction advance. Fast disappearance of MgO diffraction lines is the result of the effect of ball milling on the reaction rate. During milling, magnesium carbonate is partially decomposed and crystalline sizes are reduced to nano scale. Decomposition of magnesium carbonate leads to the generation of CO<sub>2</sub> gas. Liberation of CO<sub>2</sub> gas which fabricates micro pores decreases grain sizes and increases the contact surface between grains and forsterite formation diffusion control process.

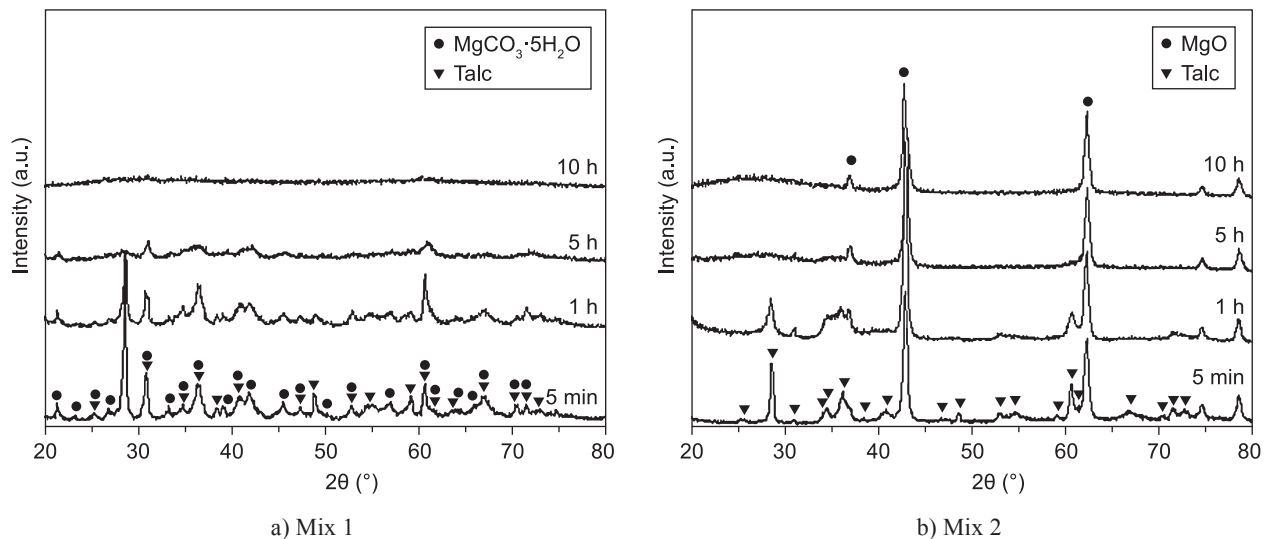


Figure 2. X-ray diffraction patterns after mechanical activation for various periods of time.

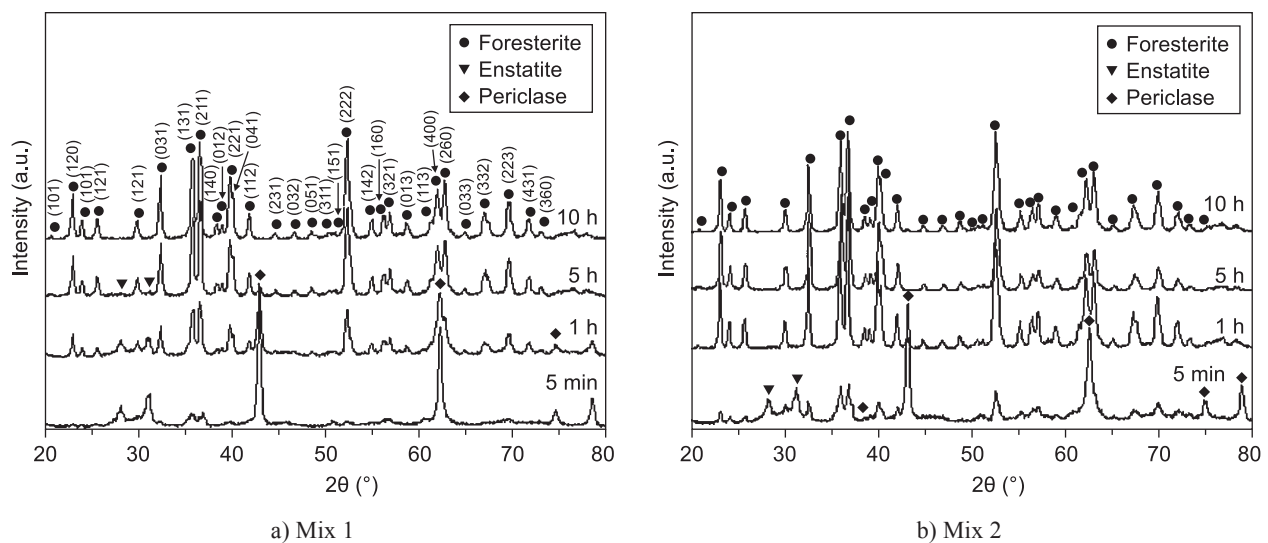


Figure 3. X-ray diffraction patterns after different mechanical activation times with subsequent annealing at 1000°C for 1 h.

On the other hand, In the case of Mix 2, for the sample milled for 5 h the peaks of periclase as well as enstatite disappeared after annealing. Fast disappearance of MgO diffraction peaks is the result of the milling effect on reaction rate. After milling for 10 h, the peaks of periclase reappeared and persisted until 10 h of mechanical activation had been accomplished after annealing. This indicates that some imperceptible  $\text{MgSiO}_3$  must have remained in the sample for the stoichiometry ratio of 2:1 for Mg:Si in the forsterite. This situation is frequently encountered in the synthesis of forsterite. Even after heating up to  $1540^\circ\text{C}$  for 5 h, which is close to the melting point of enstatite,  $\text{MgSiO}_3$  and MgO had not completely reacted to form  $\text{Mg}_2\text{SiO}_4$  [10].

Brindley and Hayami [9] showed that forsterite can be fabricated with a diffusion control mechanism. MgO initially diffuses into the surface of the  $\text{SiO}_2$  to form enstatite, and diffusion continues through this enstatite layer to form forsterite. This can be promoted by dynamically maintained high reaction interface areas as well as the short-circuit diffusion path provided by the large number of defects such as dislocations and grain boundaries induced during ball milling.

The absence of periclase and enstatite on XRD traces indicates that during mechanical activation, a homogeneous powder mixture was achieved. This result is in contrast to previous studies which reported the formation of periclase and enstatite because of lack of homogeneity of reactants [10, 20].

Figure 4 shows the effect of annealing at  $1200^\circ\text{C}$  for 1 h on structure of milled powders from Mix 1 and 2, respectively. For 5 h milled sample (Mix 1), periclase was disappeared after annealing. In contrast, enstatite was remained for samples milled for 10 h after subsequent annealing. Basically the rate of reactions

at  $1200^\circ\text{C}$  is faster than  $1000^\circ\text{C}$ . From point view of thermodynamics the free energy change of formation of  $\text{Mg}_2\text{SiO}_4$  ( $-61.145\text{ kJ/molK}$ ) is more negative than that for  $\text{MgSiO}_3$  ( $-40.542\text{ kJ/molK}$ ). Therefore the enstatite phase that formed at  $1200^\circ\text{C}$  is thermodynamically metastable, while forsterite is the more stable phase. It seems that with increasing the annealing temperature the metastable enstatite phase is formed probably because of its faster kinetics [21]. This phase appeared to be stable up to  $1600^\circ\text{C}$  [16].

For Mix 2, as can be seen in Figure 4b, the fraction of the forsterite phase increased with increasing milling time while the periclase and enstatite contents reduced after annealing, so that, only the forsterite phase was detectable in the sample milled for 5 h. Further milling up to 10 h had no significant effects on the structure or phase composition of the samples after subsequent annealing. As a result, in the presence of MgO, in comparison with  $\text{MgCO}_3$ , forsterite could be fabricated in lower milling times after subsequent annealing. This could be due to the absence of  $\text{CO}_2$  in the system in Mix 2, which caused the initial materials completely agglomerated after mechanical activation. Therefore, during mechanical activation, a homogeneous powder mixture was achieved and caused better reactivity between initial materials.

The crystallite size of the forsterite powder, which was fabricated by mechanical activation with subsequent annealing at  $1000^\circ\text{C}$  and  $1200^\circ\text{C}$ , can be determined by Williamson-Hall equation [18]. A pure nanocrystalline forsterite powder with a crystallite size of 35 nm was obtained after 10h ball milling of the first mixture and subsequent annealing at  $1000^\circ\text{C}$  for 1h. While, after 5 h of mechanical activation of the second mixture and subsequent annealing at  $1000^\circ\text{C}$  for 1 h, pure nanocrystalline forsterite was synthesized with 40 nm crystallite size.

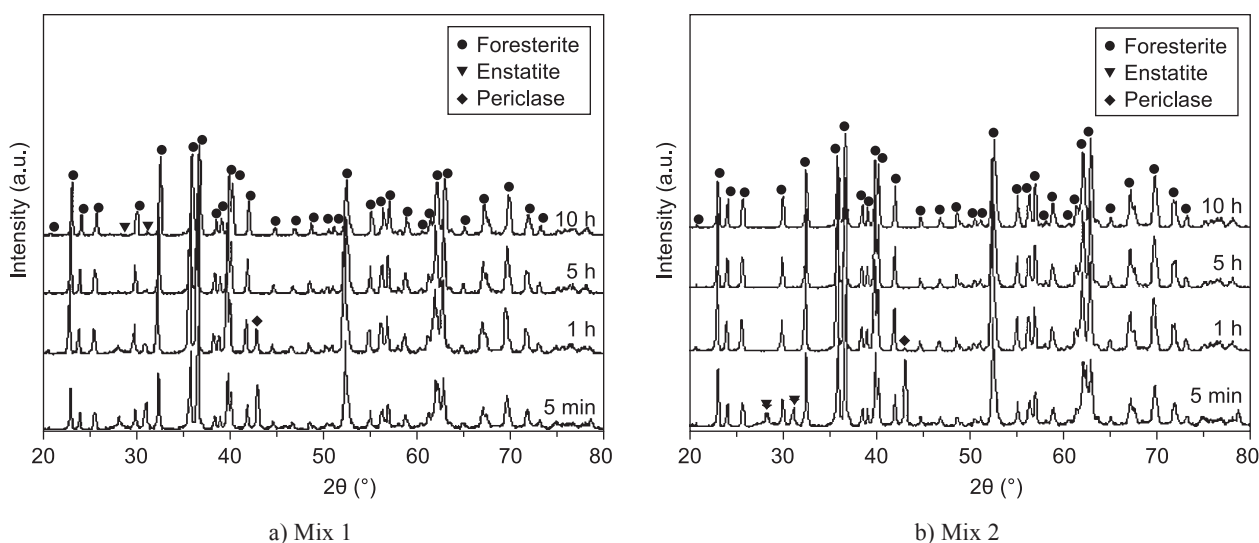


Figure 4. X-ray diffraction patterns after different mechanical activation times with subsequent annealing at  $1200^\circ\text{C}$  for 1 h.

## AAS analysis

Fe and Cr contaminations from the wear of milling media are too small to be detected by XRD. Atomic absorption spectrometry (AAS) was used to measure Fe and Cr contaminations. AAS analysis confirmed the low contamination levels of Fe and Cr in powder particles. The talc and  $\text{MgCO}_3$  are very soft materials. The amount of Fe and Cr in 10 h ball milled sample from Mix 1 were 0.0425% and 0.00125%, respectively. On the contrary, the hardness of MgO is more than  $\text{MgCO}_3$  and caused more contaminating of obtained powder in Mix 2. The amounts of Fe and Cr in the 5 h ball milled sample were 0.0734% and 0.00172%, respectively. This slight amount of contamination can have no significant effects on the properties of the final product.

## TEM evaluation

To investigate the morphology and crystallite size of prepared forsterite powder transition electron microscopy (TEM) analysis was performed. Figure 5 shows the morphological shape and size of forsterite powder crystallites after 10 h of mechanical activation of Mix 1 and 5 h of mechanical activation of Mix 2 with subsequent annealing at  $1000^\circ\text{C}$  for 1 h, respectively. It is obvious that the crystallites of forsterite obtained from both mixtures exhibit agglomerative morphologies with irregular shape. The mean crystallite size of obtained forsterite powder from Mix 1 (40 nm) was smaller than that of Mix 2 (60 nm). These results are in a good agreement with the results obtained from the Williamson-

## Hall's equation.

## SEM evaluation

The SEM micrographs of the forsterite powder prepared by 10 h of mechanical activation of the first mixture and 5 h mechanical activation of the second mixture with subsequent annealing at  $1000^\circ\text{C}$  for 1 h are shown in Figure 6, respectively. The powder particles obtained from Mix 1 were nearly uniform in size with spherical shapes (Figure 6a). The forsterite powder obtained from Mix 2 consisted of very small and highly agglomerated particles with a rounded shape (Figure 6b). As can be seen, the mean particle size of forsterite powder obtained from Mix 1 (250 nm) was smaller than that of Mix 2 (350 nm).

## CONCLUSIONS

Mechanical activation and subsequent annealing of talc and magnesium carbonate or oxide led to the formation of the single-phase nanocrystalline forsterite powder. Mechanical activation optimizes the powder mixture properties by means of combination and uttermost homogenization of the powder mass and enhances the forsterite formation rate especially in talc-MgO mixture after subsequent annealing. Although, liberation of  $\text{CO}_2$  due to the decomposition of magnesium carbonate during the mechanical activation process led to increased contact surface area and better reactivity of initial materials after subsequent annealing, in the absence of  $\text{CO}_2$  in the system (talc-MgO), the initial materials react much better and the forsterite structure

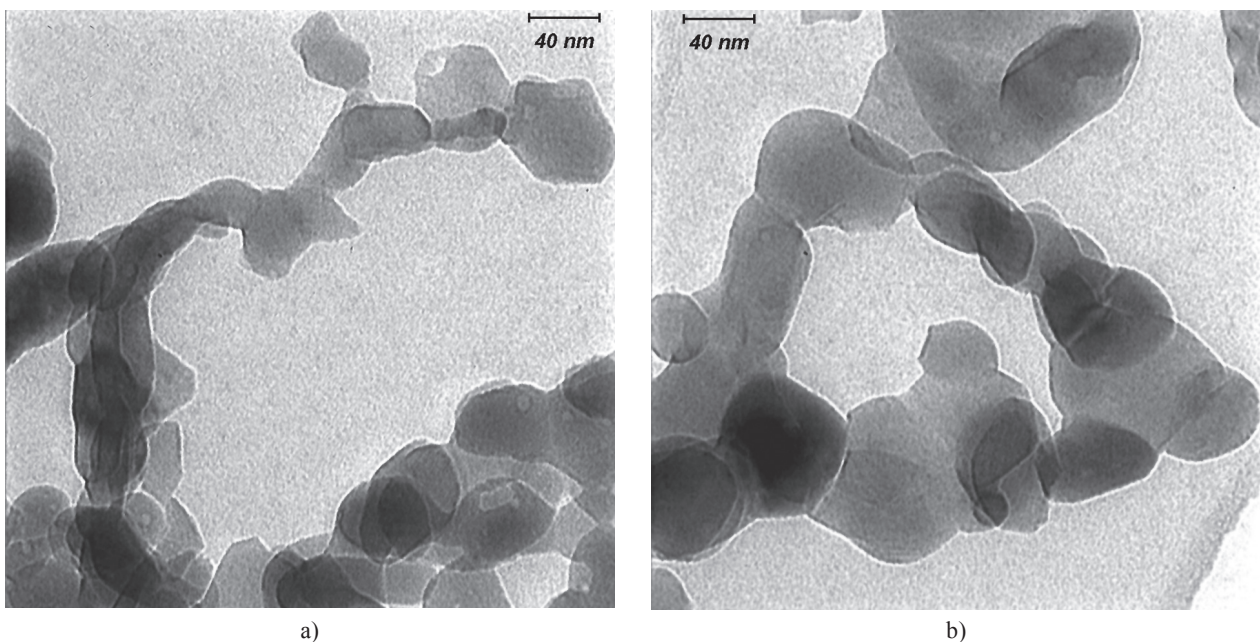
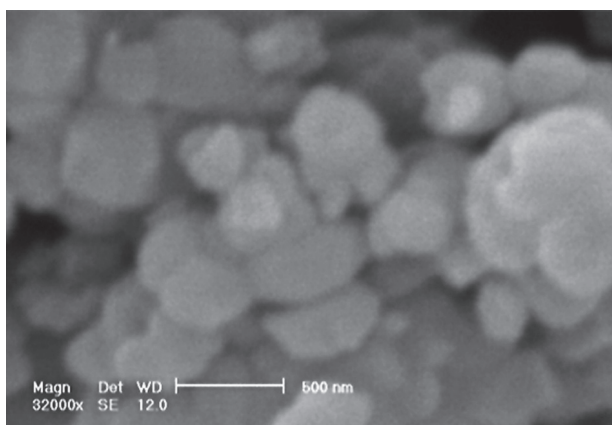


Figure 5. TEM micrograph of forsterite powder crystallites after: a) 10 h of mechanical activation of Mix 1 and b) 5 h of mechanical activation of Mix 2 with subsequent annealing at  $1000^\circ\text{C}$  for 1 h.

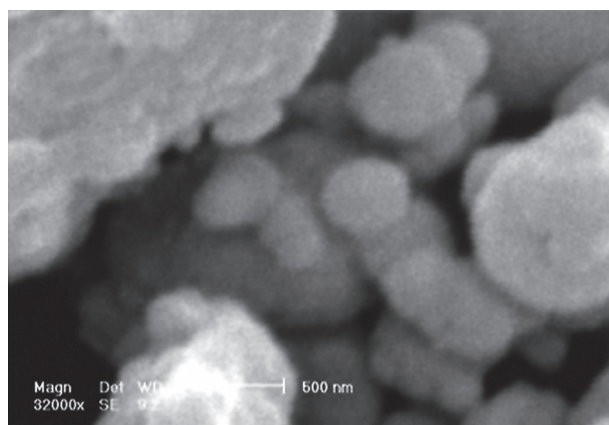
can be formed in much lower mechanical activation time. A pure nanocrystalline forsterite with a mean crystallite size of 40 nm was obtained after 10 h ball milling of Mix 1 and subsequent annealing at 1000°C for 1 h. In addition, after 5 h of mechanical activation of Mix 2 and subsequent annealing at 1000°C for 1 h, pure nanocrystalline forsterite was synthesized with 60 nm mean crystallite size.

#### References

- Suryanarayana C.: *Prog. Mater. Sci.* **46**, 1 (2001).
- Krasnowski M., Antolak A., Kulik T.: *J. Alloys Compd.* **434**, 344 (2007).
- Li F., Jiang L., Du J., Wang S.: *J. Alloys Compd.* **452**, 421 (2008).
- Maiti R., Chakraborty M.: *J. Alloys Compd.* **458**, 450 (2008).
- Chen G., Sun G. X., Zhu Z. G.: *Mater. Sci. Eng. A* **265**, 197 (1999).
- Takacs L.: *Prog. Mater. Sci.* **47**, 355 (2002).
- Kosanovic C., Stubicar N., Tomasic N., Bermanec V., Stubicar M.: *J. Alloys Compd.* **389**, 306 (2005).
- Sasikala T. S., Suma M. N., Mohanan P.: *J. Alloys Compd.* **461**, 555 (2008).
- Brindley G. W., Hayami R.: *Philos. Mag. Lett.* **12**, 505 (1965).
- Douy A., *J. Sol-Gel Sci. Technol.* **24**, 221 (2002).
- Diesperova M. I., Bron V. A., Perepelitsyn V. A., Boriskova T. I., Alekseeva V. A., Kelareva E. I.: *Refract. Ind. Ceram.* **18**, 278 (1977).
- Swanson H.E., Targe E.: *Natl. Bur. Stand.(US) Circ.* **359**, 83 (1953).
- Yamaguchi O., Nakajima Y., Shimazu K.: *Chem. Lett.* **401** (1976).
- Cunha-Duncan F. N., Bradt R. C.: *J. Am. Ceram. Soc.* **85**, 12 (1995).
- Devi P. S., Gafney H. D., Petricevi V., Alfano R.R., *J. Non-Cryst Solids.* **203**, 78 (1996).
- Kazakos A., Komarneni S., Roy R.: *Mater.Lett.* **10**, 405 (1990).
- Park D. G., Duchamp J. C., Duncan T.M., Burlitch J. M.: *Chem.Mater.* **6**, 1990 (1994).
- Williamson G. K., Hall W. H.: *Acta Metall.* **1**, 22 (1953).
- Saberi A., Alinejad B., Negahdari Z., Kazemi F., Almasi A.: *Mater.Res.Bull.* **42**, 666 (2007).
- Kiss S.J., Kostic E., Djurovic D., Boskovic S.: *Powder Technol.* **114**, 84 (2001).
- Tavangarian F., Emadi R., *J. Alloys Compd.* **485**, 648 (2009).



a)



b)

Figure 6. SEM micrograph of forsterite powder after: a) 10 h of mechanical activation of Mix 1 and b) 5 h of mechanical activation of Mix 2 and post annealing at 1000°C for 1 h.